Dense pair plasma generation by two laser pulses colliding in a cylinder channel*

Jian-Xun Liu(刘建勋)[1,2], Yan-Yun Ma(马燕云)[1,3,4,†], Tong-Pu Yu(余同普)[1,3,‡], Jun Zhao(赵军)[1], Xiao-Hu Yang(杨晓虎)[1], De-Bin Zou(邹德滨)[1], Guo-Bo Zhang(张国博)[1], Yuan Zhao(赵媛)[1], Jing-Kang Yang(杨靖康)[1], Han-Zhen Li(李汉臻)[1], Hong-Bin Zhuo(卓红斌)[1], Fu-Qiu Shao(邵福球)[1], and Shigeo Kawata[5]

[1] *College of Science, National University of Defense Technology, Changsha* 410073, *China*
[2] *College of Electronic Engineering, Wuhan* 430019, *China*
[3] *IFSA Collaborative Innovation Center, Shanghai Jiao Tong University, Shanghai* 200240, *China*
[4] *Laser Fusion Research Center, China Academy of Engineering Physics, Mianyang* 621000, *China*
[5] *Center for Optical Research and Education, Graduate School of Engineering, Utsunomiya University,* 7-1-2 *Yohtoh, Utsunomiya* 321-8585, *Japan*

(Received 28 August 2016; revised manuscript received 14 November 2016; published online 13 February 2017)

An all-optical scheme for high-density pair plasmas generation is proposed by two laser pulses colliding in a cylinder channel. Two dimensional particle-in-cell simulations show that, when the first laser pulse propagates in the cylinder, electrons are extracted out of the cylinder inner wall and accelerated to high energies. These energetic electrons later run into the second counter-propagating laser pulse, radiating a large amount of high-energy gamma photons via the Compton back-scattering process. The emitted gamma photons then collide with the second laser pulse to initiate the Breit–Wheeler process for pairs production. Due to the strong self-generated fields in the cylinder, positrons are confined in the channel to form dense pair plasmas. Totally, the maximum density of pair plasmas can be 4.60×10^{27} m^{-3}, for lasers with an intensity of 4×10^{22} W·cm^{-2}. Both the positron yield and density are tunable by changing the cylinder radius and the laser parameters. The generated dense pair plasmas can further facilitate investigations related to astrophysics and particle physics.

Keywords: pair plasma, laser pulse, simulation

PACS: 52.38.–r, 32.80.Wr **DOI:** 10.1088/1674-1056/26/3/035202

1. Introduction

Dense electron–positron pairs are demonstrated to be in the early universe, in solar atmosphere, and in inertial confinement fusion schemes using ultra-intense lasers.[1–3] One expects to uncover some mysteries of the universe by studying dense pair plasma state created via laser–plasma interactions in the laboratory.[4] For example, ultra-bright gamma ray burst is generally accepted as arising from synchrotron emission of relativistic shocks in pair plasmas.[5] The strong magnetic field required in this process should have a long life time of $\tau \geq 1000/\omega_{\rm p}$, where $\omega_{\rm p} = (4\pi e^2 n_{\rm p}/m_{\rm e})^{1/2}$ is the frequency of pair plasma, e is the charge of electron, $n_{\rm p}$ is the plasma density, $m_{\rm e}$ is the electron mass, and c is the light speed in vacuum. To initiate this process, one should reduce the threshold $(1000/\omega_{\rm p})$ as low as possible. Thus the key issue to study gamma burst in laboratory becomes to obtain high-density pair plasmas.[6]

A lot of pioneering works have been done to study positron generation and pair plasmas via laser–plasma interaction.[7–12] Since the first observation of positrons induced by laser pulses in the laboratory,[13] ultra-intense laser–plasma interaction becomes one of the most important methods for obtaining high-flux and high-density positrons. First, an indirect positron generation process is proposed, which first utilizes a low intensity laser pulse to accelerate electrons to high energies, and then strikes these electrons onto a target with high-Z nucleuses.[14] If positrons are generated via electrons colliding directly with the nucleuses, this process is named as the trident process.[15] Instead, if the interaction of electrons and nucleuses is mediated by a real photon, it is called the Bethe–Heitler (BH) process.[16,17] Recently, a direct positron generation process attracts increasing attention with the rapid development of the laser technologies. This is the multi photon Breit–Wheeler (BW) process.[18] It actually relies on three steps: firstly, one laser pulse is directly incident onto a solid target, generating energetic electron beams;[19] secondly, bright gamma rays are emitted from these energetic electrons; finally, a real photon–photon annihilation takes place and electron–positron pairs are produced. Positrons generated via this process have their unique properties, such as

*Project supported by the National Natural Science Foundation (Grant Nos. 11475260, 11305264, 11622547, 11375265, and 11474360), the National Basic Research Program of China (Grant No. 2013CBA01504), the Research Project of National University of Defense Technology, China (Contract No. JC14-02-02), and the Science Challenge Program, China (Grant No. JCKY2016212A505).

†Corresponding author. E-mail: yanyunma@126.com
‡Corresponding author. E-mail: tongpu@nudt.edu.cn

© 2017 Chinese Physical Society and IOP Publishing Ltd

high flux, high energy, and high density.[20–22] For example, by striking a 4×10^{23} W·cm^{-2} laser pulse onto an aluminum (Al) slab, it has shown that $\sim10^{10}$ positrons are generated with a maximum pair plasma density of 10^{26} m^{-3}.[23] Further increasing the intensity of the incident laser, both the yield and the maximum density become even higher. For the BH process, the required laser intensity is not as high as that of the BW process.[24] However, the achieved positron density via the BH process is much smaller and the energy conversion efficiency is lower. For the BW process, however, previous works showed that the required laser intensity is $>10^{23}$ W·cm^{-2},[22,23,25] which is one order of magnitude higher than achievable in state-of-art lasers.[26] How to obtain dense pair plasmas in present laboratories becomes an important issue.

In this paper, we report an all-optical scheme for dense pair plasmas generation by lowering the laser intensity to 10^{22} W·cm^{-2}. In the scheme, we collide two laser pulses in a cylinder channel. The first longer pulse with a spot size larger than the cylinder inner radius is utilized to extract and accelerate electrons in the channel. When these electrons are accelerated to high energies, they collide with the second counter-propagating shorter laser pulse to emit strong gamma radiations via the Compton back-scattering process. The radiated gamma photons further interact with the second laser photons to initiate the multi-photon BW process. Finally, high-flux and high-density pair plasmas are produced. Our two-dimensional (2D) practice-in-cell (PIC) simulations indicate that the final pair plasma density is up to 4.60×10^{27} m^{-3}, though the peak intensity of the laser pulse used in the simulation is only 4×10^{22} W·cm^{-2}. We also study the parametric influences of the laser and channel size on the positrons generation and an optimal channel radius is obtained. The generated dense pair plasma may facilitate investigations related to astrophysics and particle physics.

2. Simulation model

The simulations are carried out by using the relativistic PIC code EPOCH2D.[25,27] Here, we only consider the BW process for positron generation as the laser intensity is ultra-intense. For simplicity, the BW process can be expressed by $\gamma_r+n\gamma_l\rightarrow e^-+e^+$, where γ_r is a radiated gamma photon by an energetic electron and γ_l is a laser photon. Provided that the energy of generated electrons and positrons are high enough, a cascade may occur. In our scheme, two counter-propagating laser pulses with different durations are utilized, as schematically shown in Fig. 1. The shorter one transmits from the left to the right with a pulse duration of 15 fs and a spot radius of 2 μm. The longer pulse propagates oppositely with a duration of 40 fs and a spot radius of 4 μm. Here, the longer pulse is expected to extract and accelerate electrons from the channel inner wall, while the shorter one provides laser photons for the Compton back-scattering and the BW process. Both of the two laser pulses have a Gaussian profile and are circular polarized with a peak intensity of $I=4\times10^{22}$ W·cm^{-2} and a wave length of $\lambda_0=1$ μm. The corresponding dimensionless maximum amplitude of the laser electric field is $a_0=[I/(2.74\times10^{18})]^{1/2}\approx120$.[28] The simulation box size is $35\lambda_0$ long and $20\lambda_0$ wide, divided into 1725×1000 cells with each cell size of $0.02\lambda_0\times0.02\lambda_0$. As the laser–plasma interaction is highly nonlinear in our case and the interaction duration is very short. The plasma temperature increases significantly in a few laser cycles. The corresponding Debye wavelength and the relativistic corrected skin length become much larger, making it comparable with our cell size. An Al cylinder channel is located between $0<x<35\lambda_0$ and $2\lambda_0<|y|<4\lambda_0$. Considering the ultra-high laser intensities in our scheme, the cylinder is assumed fully ionized (Al^{13+}) with an initially electron density of $700n_c$, where $n_c=m_e\omega_0^2/4\pi e^2$ is the critical density corresponding to the incident laser pulses, and $\omega_0=2\pi/T_0$ is the laser frequency.[29,30] In each cell of plasma, 40 macroparticles are initially set.

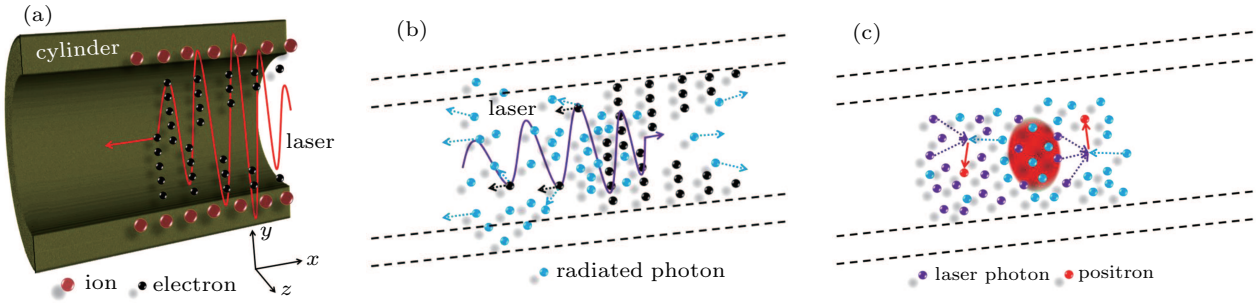


Fig. 1. (color online) Schematics of two circularly polarized laser pulses colliding in a cylinder channel. Electrons are firstly extracted out of the cylinder inner wall and accelerated to high energy by the laser pulse (a), and then radiate high energy gamma photons in the counter-propagating pulse via the Compton back-scattering process (b). The radiated photons further interact with the laser photons to generate copious positrons (c).

3. Simulation results

When the longer laser pulse is incident onto the cylinder channel, electrons at the cylinder inner wall are firstly extracted out by the transverse electric field E_y. Neglecting the charge-separation field, the energy an electron acquired from E_y can be estimated by $\mathrm{d}E_{\mathrm{kin}}/\mathrm{d}s = -eE_y$, where E_{kin} is the electron kinetic energy and s is the displacement of the test electron in the y direction.[31] After electrons are extracted out, the $\boldsymbol{V} \times \boldsymbol{B}$ force will turn these electrons in the laser propagating direction.[32] Meanwhile, the longitudinal component of the electric field arising from the transverse magnetic (TM) modes[33] and the laser ponderomotive force[34–36] will continue to accelerate the electrons to high energies. In our scheme, two counter-propagating laser pulses are incident onto the cylinder from the openings at the same time, as shown in Fig. 2(a). As the spot radiuses of the two laser pulses are 2 μm and 4 μm respectively and the cylinder inner radius is set only 2 μm, a lot of electrons are extracted from the inner wall of the channel by the pulses, especially by the one with larger spot size. The transverse electric field E_y responsible for extracting electrons out of the cylinder inner wall can be up to $\sim 10^{14}$ V/m. It is noted from Fig. 2(b) that the extracted electrons distribute firmly according to the local laser electric fields distribution. The electron density stripe interval is equal to the laser wavelength.

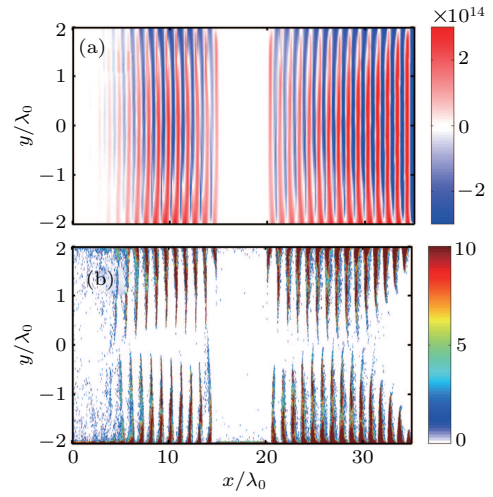


Fig. 2. (color online) (a) The transverse laser field E_y in unit of V/m and (b) the electron number density distribution in unit of n_c at $t = 15T_0$.

As the two laser pulses propagate deep into the channel, more electrons are extracted out. On the one hand, these electrons are accelerated together with the incident laser pulse and move towards the counter-propagating laser pulse. On the other hand, they are centralized to the longitudinal axis, where the peak laser intensity lies. Both the acceleration and the centralization of these high-flux electrons are of significant importance in the positron generation via the BW process, due to their potentials for high-energy-density gamma photons emission.

Figure 3 shows the divergences and spectra of electrons and photons. At an early time, e.g., $t = 15T_0$, electrons transmit in the channel with a small divergence along the laser pulse by which they are extracted out. Electrons extracted out by the shorter pulse are in the x direction, while those extracted by the longer pulse are in the $-x$ direction. As the two laser pulses propagating deeply into the cylinder, more electrons are extracted out at $t = 22T_0$. At the same time, the divergence of electrons becomes larger. This is due to the strong transverse force from the electric field E_y. The transverse force gets stronger as electrons moving close to the laser axis. At $t = 32T_0$, these electrons run into the opposite laser pulse. As they suffer an opposite force from the opposite laser pulse, electrons on either side of the cylinder will be decelerated, some of which even change their directions. Electrons only dominate in the $-x$ direction, as noted in Fig. 3(a). It can be seen from Fig. 3(c) that electron energies increase till pulses collision at $t = 22T_0$. The cutoff energy of electrons at this time is ~ 6 GeV. The high energy part of the electron spectrum resembles a relativistic Maxwellian distribution, whose effective temperature is ~ 1.14 GeV. However, after pulses collision at $t = 22T_0$, the cutoff energy of electrons decreases greatly. Besides the opposite force electrons suffer, most electron energies are passed to gamma photons via the Compton back-scattering process. When the shorter pulse passes through the longer one, the cutoff energy of electrons increases again. At $t = 42T_0$, the cutoff energy is only a little higher than that at $t = 32T_0$. Though electrons only suffer the accelerating force from one laser, the increased energies are partially lost via radiations. Figure 3(b) shows divergences of photons at different times. Taking the third dimension into account, we have multiplied the numbers of generated photons and positrons by a factor of $\sqrt{2}r$ so that we can compare it with the real particle numbers in the 3D case.[21,37] Here, r is the laser spot size. At $t = 15T_0$, when electrons are extracted out of the inner wall of the cylinder, there are already a lot of photons radiated. These photons dominate in directions of each laser pulse. As the two laser pulses propagate deep into the cylinder, the photon divergence gets larger, while the photon number increases quickly. When electrons run into the opposite propagating laser pulse, their divergence gets larger as shown in Fig. 3(a), which induces larger photon divergence. Electrons colliding with the opposite propagating laser pulse increase the probability of Compton back-scattering. Photons radiated at an early time before pulses collision have a low energy (Fig. 3(d)). Photon energy increases as electrons are accelerated in the channel. At $t = 42T_0$, the cutoff energy is ~ 3 GeV with mean photon energy ~ 6.05 MeV, which is much higher than the positron generation threshold $E_0 = 2mc^2 \approx 1.022$ MeV. These high-energy photons can generate high-energy electron-positron pairs by further interacting with the laser photons via the BW process. If the energy of pairs is still high enough to radiate photons with energy $> E_0$, thus a cascade for pair generation occurs.

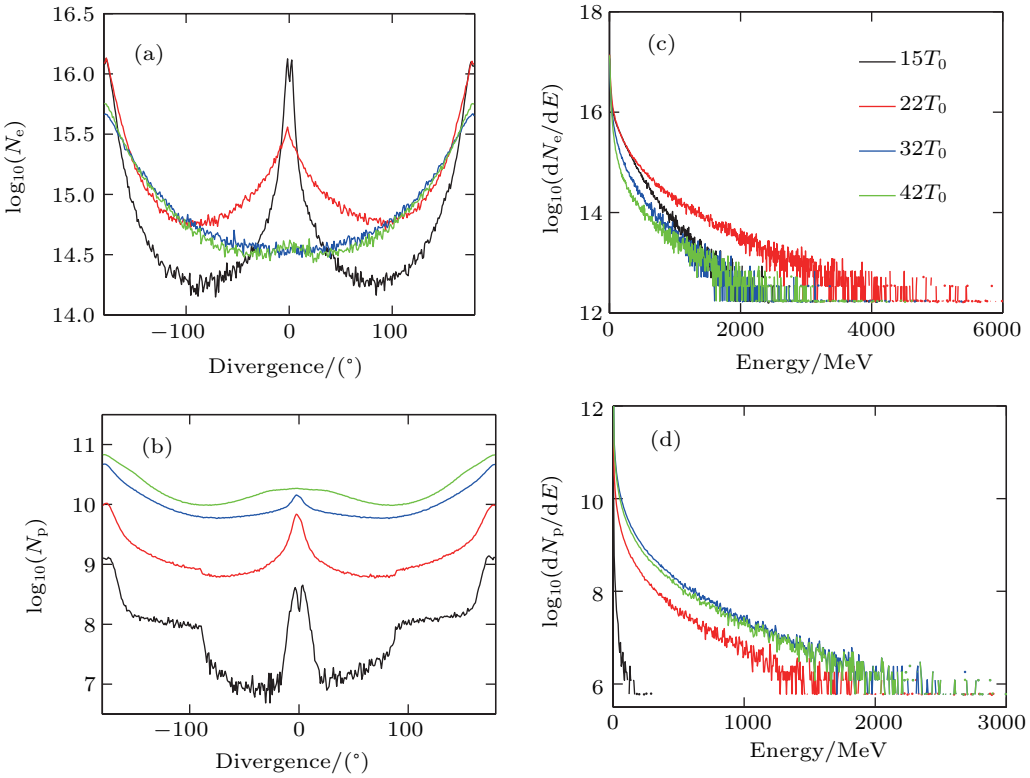


Fig. 3. (color online) Divergences ((a) and (b)) and spectra ((c) and (d)) of extracted electrons ((a) and (c)) and radiated gamma photons ((b) and (d)) at $t = 15T_0$, $22T_0$, $32T_0$, and $42T_0$, respectively.

For more details, figure 4 shows the number density and energy density of photons. At $t = 15T_0$, when electrons are extracted and accelerated, the number density distribution and energy density distribution of photons correspond to the distribution of electrons as compared the Fig. 2(b) with Figs. 4(a) and 4(d). The maximum photon number density can be tens of n_c, while the energy density is up to 10^{15} J/m^3. These high-energy-density photons are very beneficial to positrons generation via the BW process. However, there are no positrons generated at this time. For positrons generation via the BW process, the controlling parameter is $\chi \approx (\hbar\omega_\gamma/2m_ec^2)|\boldsymbol{E}_\perp + \boldsymbol{k}\times c\boldsymbol{B}|$, where $\boldsymbol{k}$ is the direction of gamma photons, $\boldsymbol{E}_\perp$ is the electric field component perpendicular to $\boldsymbol{k}$, and $\boldsymbol{B}$ is the magnetic field. At $t = 15T_0$, the two laser pulses have not collided with each other, and electrons/photons transmit with each pulse separately, which means the electric field $\boldsymbol{E}_\perp$ is almost cancelled by $\boldsymbol{k}\times c\boldsymbol{B}$, resulting in $\chi \approx 0$. When pulse collision begins at $t = 22T_0$, both the number density and the energy density are greatly increased as shown in Figs. 4(b) and 4(d). The photon energy density can be up to 10^{17} J/m^3 at this time. These high-energy-density photons distribute in the collision region within the channel. At $t = 32T_0$, the extracted electrons almost run into the counter-propagating pulse, and the Compton back-scattering process is greatly enhanced. It is noted from Figs. 4(c) and 4(f) that the photon number density mainly distributes at the cylinder inner wall in the collision region, and the maximum density is increased to hundreds of n_c. However, the high-energy-density photons are still centralized in the center of the channel in the collision region. Components of $\boldsymbol{E}_\perp$ and $\boldsymbol{k}\times c\boldsymbol{B}$ are almost in the same direction, which provides an optimal controlling parameter χ for positron generation via the BW process. The positron generation is greatly enhanced.

When the two laser pulses collide with each other at $t = 22T_0$, the controlling parameter χ increases suddenly. It can be seen from Fig. 5(a) that copious positrons are generated at this time with a maximum density around the critical density n_c. Subsequently at $t = 42T_0$, the positron yield can be increased by two orders of magnitude with the maximum density up to a few n_c. These positrons generated via the BW process can be marked as two parts: laser photons of the shorter pulse interacting with photons radiated from electrons accelerated by the longer pulse and laser photons of the loner pulse interacting with photons radiated from electrons accelerated by the shorter pulse. The generated positrons are mainly centralized in the channel, forming dense pair plasmas. If we count only positrons in the channel, 87.2% of the generated positrons are confined in the channel, which is useful for investigations of solar atmosphere[38] and others related to astrophysics. When firstly generated at $t = 22T_0$, positrons are uniformly distributed in the channel, which can be seen from Fig. 5(a). As the interaction continues, the generated positrons are pushed by the longer pulse, as compared the number density distribution of positrons in Fig. 5(b) with 5(c). Figure 5(d)

shows the spectra of positrons in the channel. It can be seen from Fig. 5(d) that the cutoff energy of positrons is ~ 500 MeV with an average temperature ~ 154 MeV at $t = 42T_0$. However, the cutoff energy at $t = 42T_0$ increases no longer as compared to $t = 32T_0$. On the contrary, the average temperature decreases, as shown in Fig. 5(d).

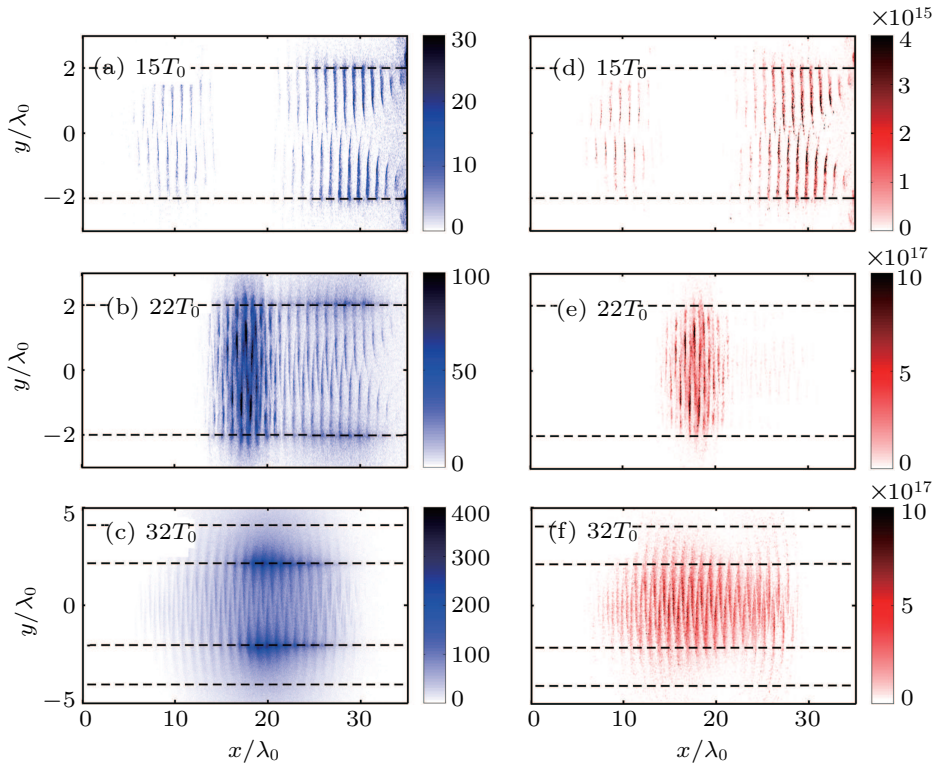


Fig. 4. (color online) Distributions of the photon number density (blue) in unit of n_c and the photon energy density (red) in unit of J/m^3 at $t = 15T_0$ ((a) and (d)), $22T_0$ ((b) and (e)), and $32T_0$ ((c) and (f)), respectively.

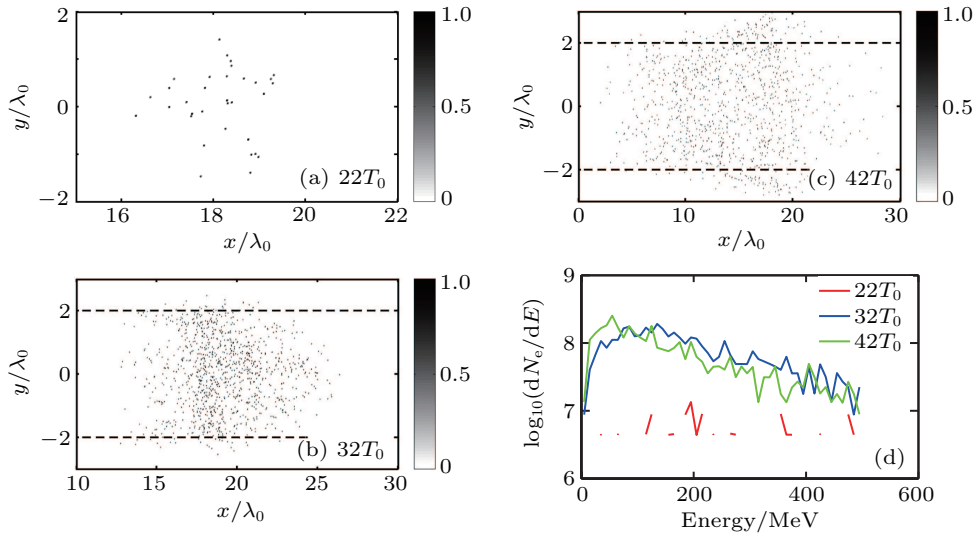


Fig. 5. (color online) Positron density in unit of n_c at $t = 22T_0$ (a), $32T_0$ (b), $42T_0$ (c), and the spectra of positrons in the channel (d).

To uncover the underlying physics, figure 6 shows the self-generated field in the channel at $t = 32T_0$. As we can see, positrons are distributed in the strong laser field and suffer a strong accelerating force. As most positrons are generated via the shorter pulse colliding with radiated gamma photons from electrons extracted by the longer pulse, the force from the longer pulse pushes positrons in the $-x$ direction. However, the field as marked by 1 in Fig. 6(d) provides a force in the x direction, which decelerates positrons from accelerating out of the left opening. It is noted from Figs. 6(b) and 6(e) that the strong transverse electric field E_y forms a trap attached to the cylinder inner wall. Positrons are trapped in the cylinder channel instead of transmitting transversely out of the

channel. When moving along the channel, positrons suffer a strong transverse force from the magnetic field B_z, as shown in Figs. 6(c) and 6(f). The force of $\boldsymbol{V} \times \boldsymbol{B}$ changes the direction of positrons, and prevents positrons from accelerating out of the channel. This is the reason why the cutoff energy of positron no longer increases as shown in positron spectrum (Fig. 5(d)). Due to the electric field E_y and the transverse magnetic field B_z, positrons are confined in the cylinder channel, forming dense pair plasmas. At $t = 42T_0$, the maximum density of positrons is $\sim 4.60 \times 10^{27}$ m^{-3}, which is about $4.18n_c$.

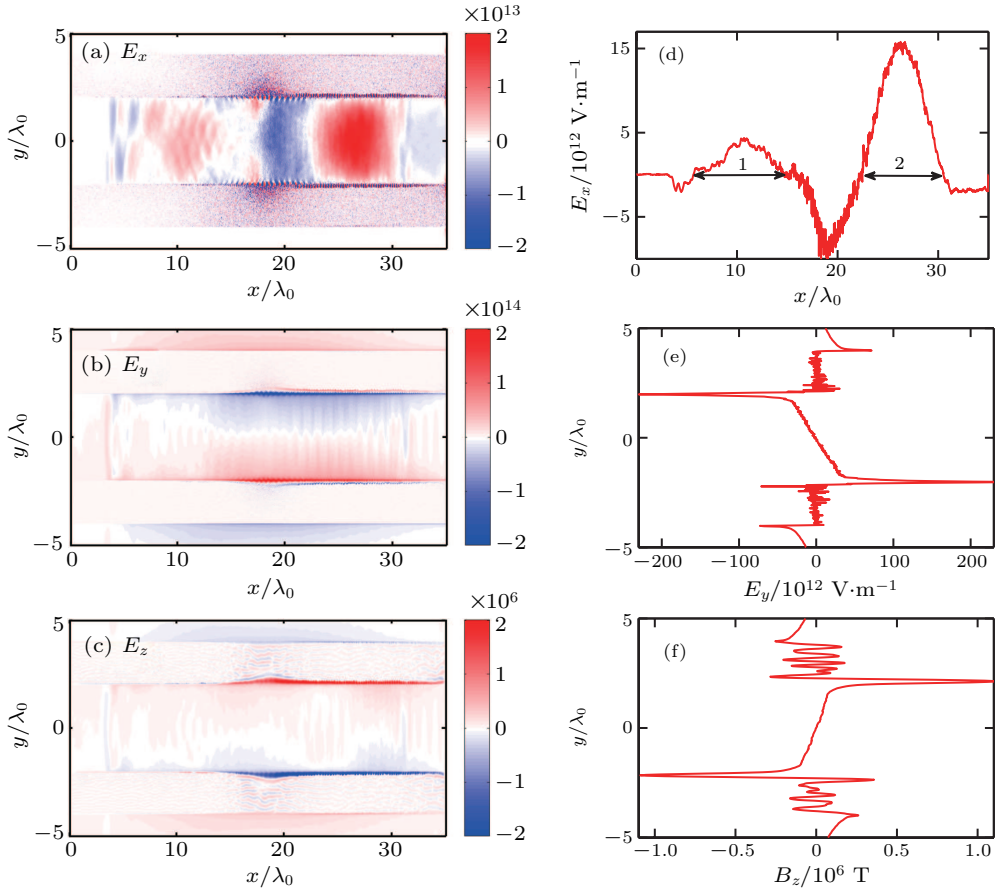


Fig. 6. (color online) Distributions of the field E_x (a), E_y (b), B_z (c) in unit of V/m and T, and their profiles along the x axis (d) and $x = 20\lambda_0$ ((e) and (f)) at $t = 32T_0$, respectively. Here, the laser field has already been cancelled out by averaging it every laser period.

4. Discussion

To investigate influences of the channel radius on positron generation, we carry out a series of simulations with different radiuses. Figures 7(a) and 7(c) show the electron energy density in simulations of channel radius 4 μm and 1 μm at $t = 15T_0$. When the channel radius is large (e.g. 4 μm), fewer electrons are extracted out of the channel inner wall with smaller energy density. When the pulses collision is initiated, electrons extracted out may not run into the counter-propagating pulse, by passing the edge of the pulse. Provided the channel radius large enough, it is believed that no electrons will be extracted out. Thus, no photons are radiated via the Compton back-scattering process, resulting in no positron generation. When the channel radius is 1 μm (Fig. 7(c)), high-energy-density electrons are extracted out and almost fill in the channel. In a channel with smaller radius, high-energy-density electrons will initiate strong gamma photons emission. Taking the laser pulse into account, it is noted from Fig. 7(b) that the laser transverse field decreases quickly as the channel radius gets smaller than 2 μm. If the channel radius is too small, most laser energy is consumed by extracting and accelerating electrons, resulting in a weak laser intensity at the time of pulses collision. Firstly, collision of electrons with a weak laser pulse weakens the Compton back-scattering process, which reduces the number and energy of radiated gamma photons. Secondly, in the BW process, the quality of laser photons also determines positron generation. A weak laser pulse is undesirable for high-flux positron generations via the BW process. In the end, though the energy density of electrons in the channel is very high, the positron yield decreases as the channel radius gets smaller than 2 μm. In our scheme, a channel radius of 2 μm is optimal for positron generations with the given laser focus spot, as seen in Fig. 7(d). A smaller or a larger channel radius will induce fewer positrons generation.

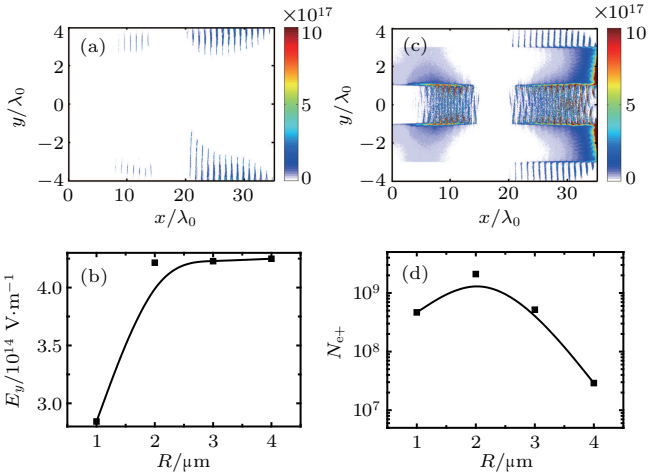


Fig. 7. (color online) The electron energy density distribution at $t = 15T_0$ in simulations with channel radiuses of 4 μm (a) and 1 μm (c). (b) The laser field E_y at $t = 32T_0$ as a function of the cylinder radius. (d) The positron yield at $t = 32T_0$ as a function of the channel radius.

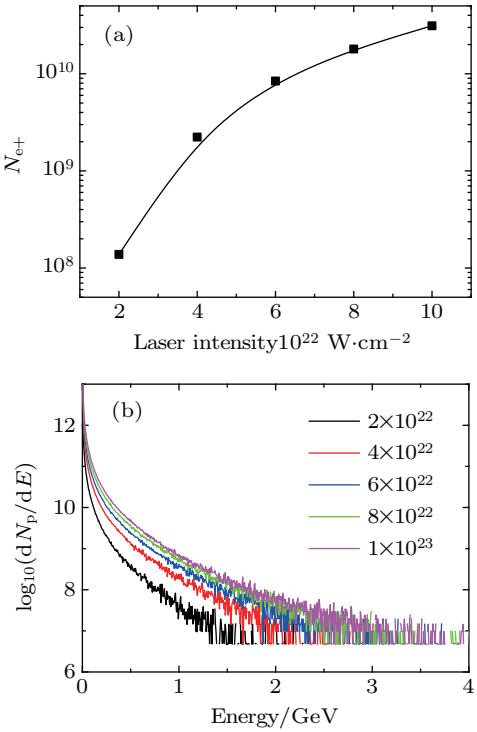


Fig. 8. (color online) (a) The positron yield as a function of the laser intensity and (b) photon spectra at $t = 32T_0$ in simulations with different laser intensity (W·cm^{-2}).

Besides, positron generation is firmly related to the laser intensity.[39] Figure 8(a) shows the positron yield as a function of the laser intensity. In these simulations, the channel radius is 2 μm and the other parameters of the cylinder and laser pulses are also kept unchanged except the laser intensity. It can be seen that the positron yield increases by more than 2 orders of magnitude as the laser intensity increases from 2×10^{22} W·cm^{-2} to 1×10^{23} W·cm^{-2}. The maximal density can be increased from 2.39×10^{27} m^{-3} to 9.28×10^{27} m^{-3}. On the one hand, increasing the laser intensity can provide high electric field for extracting and accelerating electrons, which results in high-flux and high-energy electrons in the channel. These high-flux and high-energy electrons directly induce high-flux and high-energy photon radiations. Figure 8(b) shows the spectra of radiated photons at $t = 32T_0$. It is noted that both the cutoff energy and the number of radiated photons are increased as the laser intensity increases. When the laser intensity is 2×10^{22} W·cm^{-2}, the cutoff energy of photons is 2 GeV. If the laser intensity is increased to 1×10^{23} W·cm^{-2}, the cutoff energy of photons is greater than 4 GeV. The yield of radiated photons is increased by more than 1 order of magnitude. On the other hand, high laser intensity also provides high-energy-density laser photons in the BW process to enhance positron generations. Increasing the laser peak intensity can also increase the positron energy. The cutoff energy of positrons is increased by 100 MeV when the laser peak intensity is increased from 2×10^{22} W·cm^{-2} to 1×10^{23} W·cm^{-2}. This demonstrates that the yield and the energy of positrons are tunable by controlling the laser intensity. In real, however, it seems difficult to raise the laser intensity greater than 10^{23} W·cm^{-2} under current laboratory conditions.

5. Conclusion

A new scheme for dense pair plasma generation is proposed via two colliding laser pulses at an intensity of 4×10^{22} W·cm^{-2}. The longer pulse is utilized to extract electrons from the inner wall of the cylinder and accelerate them to high energy in the cylinder channel. The shorter pulse provides fields for high-energy and high-flux photon radiations and laser photons for positron generation via the BW process. When electrons run into the opposite laser pulse, gamma photon radiations via the Compton back-scattering of electrons are quickly initiated, and the cross section for radiated photons interaction with the laser photons is greatly increased. The BW process is greatly enhanced in the cylinder channel with high-flux positron generations. When the two pulses transmit through the channel, the self-generated field can confine positrons in the channel to form dense pair plasmas. Finally, under the present available laser intensity of 4×10^{22} W·cm^{-2}, dense pair plasmas with a maximum density of 4.60×10^{27} m^{-3} are obtained. Provided a constant laser spot size, the cylinder radius has significant influences on positron generation by affecting the number and energy of extracted electrons. It is also found that in our scheme, an optimal cylinder radius for positron generation is 2 μm, while a larger radius will induce fewer electrons extracted out and a smaller one prevents electrons from acceleration. When the laser intensity is increased, the positron generation is enhanced because of more electrons extracted out and higher energies they acquire. The obtained dense pair plasmas can further facilitate many investigations in the future, such as gamma burst

in universe, the study of black hole, and even physics in inertial confinement fusion.

Acknowledgment

The authors wish to acknowledge CFSA at University of Warwick for allowing usage of EPOCH.

References

[1] Ali Shan S, El-Tantawy S A and Moslem W M 2013 *Phys. Plasmas* **20** 082104
[2] Ruffini R, Vereshchagin G and Xue S 2010 *Phys. Rep.* **487** 1
[3] Khan S A and Wazir Z 2013 *Chin. Phys. B* **22** 025201
[4] Foster J M, Wilde B H, Rosen P A, Williams R J R, Blue B E, Coker R F, Drake R P, Frank A, Keiter P A and Khokhlov A M 2005 *Astrophys. J. Lett.* **634** L77
[5] Sarri G, Poder K, Cole J, Schumaker W, Piazza A D, Reville B, Doria D, Gizzi L A, Grittani and Kar S 2015 *Nat. Commun.* **6** 6747
[6] Greaves R G, Tinkle M D and Surko C M 1994 *Phys. Plasmas* **1** 1439
[7] Chang H X, Qiao B, Xu Z, Xu X R, Zhou C T, Yan X Q, Wu S Z, Borghesi M, Zepf M and He X T 2015 *Phys. Rev. E* **92** 053107
[8] Jirka M, Klimo O, Bulanov S V, Esirkepov T Z, Gelfer E, Bulanov S S, Weber S and Korn G 2016 *Phys. Rev. E* **93** 023207
[9] Nakamura T and Hayakawa T 2015 *Phys. Plasmas* **22** 083113
[10] Shen B and Meyertervehn J 2002 *Phys. Rev. E* **65** 016405
[11] Jiang M, Xie B S, Sang H B and Li Z L 2013 *Chin. Phys. B* **22** 100307
[12] Zhu X L, Yu T P, Sheng Z M, Yin Y, Turcu I C E and Pukhov A 2016 *Nat. Commun.* **7** 13686
[13] Burke D L, Field R C, Horton-Smith G, Spencer J E, Walz D, Berridge S C, Bugg W M, Shmakov K, Weidemann A W and Bula C 1997 *Phys. Rev. Lett.* **79** 1626
[14] Yan Y H, Wu Y, Dong K, Zhang B, Zhao Z, Yao Z and Gu Y 2014 *Eur. Phys. J. D* **68** 4
[15] Gahn C, Tsakiris G, Pretzler G, Witte K, Thirolf P, Habs D, Delfin C and Wahlström C G 2002 *Phys. Plasmas* **9** 987
[16] Williams G J, Pollock B B, Albert F, Park J and Chen H 2015 *Phys. Plasmas* **22** 093115
[17] Sarri G, Schumaker W, Di Piazza A, Vargas M, Dromey B, Dieckmann M E, Chvykov V, Maksimchuk A, Yanovsky V and He Z 2013 *Phys. Rev. Lett.* **110** 255002
[18] Yan Y H, Zhang B, Wu Y, Dong K, Yao Z and Gu Y 2013 *Phys. Plasmas* **20** 103114
[19] Liu J X, Ma Y Y, Zhao J, Yu T P, Yang X H, Gan L F, Zhang G B, Yan J F, Zhuo H B, Liu J J, Zhao Y and Kawata S 2015 *Phys. Plasmas* **22** 103102
[20] Ridgers C P, Brady C S, Duclous R, Kirk J, Bennett K, Arber T, Robinson A and Bell A 2012 *Phys. Rev. Lett.* **108** 165006
[21] Luo W, Zhu Y B, Zhuo H B, Ma Y Y, Song Y M, Zhu Z C, Wang X D, Li X H, Turcu I C E and Chen M 2015 *Phys. Plasmas* **22** 063112
[22] Zhu X L, Yin Y, Yu T P, Shao F Q, Ge Z Y, Wang W Q and Liu J J 2015 *New J. Phys.* **17** 053039
[23] Ridgers C P, Brady C S, Duclous R, Kirk J, Bennett K, Arber T and Bell A 2013 *Phys. Plasmas* **20** 056701
[24] Chen H, Wilks S C, Bonlie J D, Liang E P, Myatt J, Price D F, Meyerhofer D D and Beiersdorfer P 2009 *Phys. Rev. Lett.* **102** 105001
[25] Brady C, Ridgers C, Arber T and Bell A 2013 *Plasma Phys. Control. Fusion* **55** 124016
[26] Yu T P, Yu W, Shao F Q, Luan S X, Zou D B, Ge Z Y, Zhang G B, Wang J W, Wang W Q, Li X H, Liu J X, Ouyang J M and Wong A Y 2015 *J. Appl. Phys.* **117** 023105
[27] Arber T D, Bennett K, Brady C S, Lawrence-Douglas A and Ramsay M G 2015 *Plasma Phys. Control. Fusion* **57** 113001
[28] Ji L L, Pukhov A, I Yu K, Shen B F and Akli K 2014 *Phys. Rev. Lett.* **112** 145003
[29] Yu T P, Pukhov A, Shvets G and Chen M 2010 *Phys. Rev. Lett.* **105** 065002
[30] Ma Y Y, Kawata S, Yu T P, Gu Y Q, Sheng Z M, Yu M Y, Zhuo H B, Liu H J, Yin Y, Takahashi K, Xie X Y, Liu J X, Tian C L and Shao F Q 2012 *Phys. Rev. E* **85** 046403
[31] Ma Y Y, Sheng Z M, Li Y T, Chang W W, Yuan X H, Chen M, Wu H C, Zheng J and Zhang J 2006 *Phys. Plasmas* **13** 110702
[32] Zou D B, Hu L X, Wang W Q, Yang X H, Yu T P, Zhang G B, Ouyang J M, Shao F Q and Zhuo H B 2015 *High Energy Density Phys.* **18** 1
[33] Yi L Q, Pukhov A, Luu-Thanh P and Shen B F 2016 *Phys. Rev. Lett.* **116** 115001
[34] Hu L X, Yu T P, Shao F Q, Zou D B and Yin Y 2015 *Phys. Plasmas* **22** 033104
[35] Zou D B, Zhuo H B, Yu T P, Wu H C, Yang X H, Shao F Q, Ma Y Y, Yin Y and Ge Z Y 2015 *Phys. Plasmas* **22** 023109
[36] Yu T P, Hu L X, Yin Y, Shao F Q, Zhuo H B, Ma Y Y, Yang X H, Luo W and Pukhov A 2014 *Appl. Phys. Lett.* **105** 114101
[37] Liu J J, Yu T P, Yin Y, Zhu X L and Shao F Q 2016 *Opt. Express* **24** 015978
[38] Ni L, Kliem B, Lin J and Wu N 2015 *Astrophys. J.* **799** 79
[39] Liu J X, Ma Y Y, Yu T P, Zhao J, Yang X H, Gan L F, Zhang G B, Zhao Y, Zhang S J, Liu J J, Zhuo H B, Shao F Q and Kawata S 2016 *Plasma Phys. Control. Fusion* **58** 125007